

Beam Energy dependence of Light Nuclei Production in Au+Au Collisions

Wenbin Zhao,^{1,2,3,4} Chun Shen,^{5,6} Che Ming Ko,⁷ Quansheng Liu,^{1,2} and Huichao Song^{1,2,3}

¹*Department of Physics and State Key Laboratory of Nuclear Physics and Technology, Peking University, Beijing 100871, China*

²*Collaborative Innovation Center of Quantum Matter, Beijing 100871, China*

³*Center for High Energy Physics, Peking University, Beijing 100871, China*

⁴*Institute of Particle Physics and Key Laboratory of Quark and Lepton Physics (MOE), Central China Normal University, Wuhan, Hubei 430079, China*

⁵*Department of Physics and Astronomy, Wayne State University, Detroit, MI 48201, USA*

⁶*RIKEN BNL Research Center, Brookhaven National Laboratory, Upton, NY 11973, USA*

⁷*Department of Physics and astronomy, Cyclotron Institute, a Texas A&M University, College Station, TX 77843, USA*

(Dated: October 13, 2021)

We study in the coalescence model the collision energy dependence of (anti-)deuteron and (anti-)triton production in the most central Au+Au collisions at $\sqrt{s_{NN}} = 7.7, 11.5, 19.6, 27, 39, 62.4$ and 200 GeV. The needed phase-space distribution of nucleons at the kinetic freeze-out is generated from a new 3D hybrid dynamical model (iEBE-MUSIC) by using a smooth crossover equation of state (EoS) without a QCD critical point. Our model calculations predict that the coalescence parameters of (anti-)deuteron ($B_2(d)$ and $B_2(\bar{d})$) decrease monotonically as the collision energy increases, and the light nuclei yield ratio $N_t N_p / N_d^2$ remains approximately a constant with respect to the collision energy. These calculated observables fail to reproduce the non-monotonic behavior of the corresponding data from the STAR Collaboration. Without including any effects of the critical point in our model, our results serve as the baseline predictions for the yields of light nuclei in the search for the possible QCD critical points from the experimental beam energy scan of heavy ion collisions.

PACS numbers: 25.75.Ld, 25.75.Gz, 24.10.Nz

I. INTRODUCTION

One of the primary goals of the experiments at the Relativistic Heavy Ion Collider (RHIC) is to explore and map out the phase structure of QCD [1–10]. In particular, the search for the conjectured critical point in the QCD phase diagram has attracted much interest in the past ten years [8–26]. Experiments at the RHIC Beam Energy Scan (BES) program have already found some intriguing results that might be related to the critical phenomenon in QCD matter. For example, the cumulant ratio $k\sigma^2$ of the kthosis κ and variance σ^2 of the (net) proton multiplicity distribution obviously deviates from the Poisson distribution expected from statistical fluctuations and shows a non-monotonic behavior at lower collision energies [27]. Also, the Gaussian emission source radii difference ($R_{out}^2 - R_{side}^2$) extracted from two-pion interferometry measurements is found to have a non-monotonic dependence on the collision energy with a maximum value at around $\sqrt{s_{NN}} = 20$ –40 GeV [28–30]. Furthermore, the measured yield ratio $N_t N_p / N_d^2$ of proton, deuteron and triton in central Au+Au collisions clearly shows a non-monotonic behavior in its collision energy dependence with a peak around $\sqrt{s_{NN}} = 20$ GeV [31].

Besides studying the signatures of critical fluctuations in heavy ion collisions, it is also important and necessary to systematically investigate and understand the noncritical and/or thermal fluctuations that are present in these collisions as they provide the background against which the signals can be identified and used to locate the po-

sition of the possible critical point in the QCD phase diagram [8, 9, 32–39]. However, because of the many complicated processes involved in realistic heavy-ion collisions, it is difficult to obtain clean baseline contributions to observables in these collisions. For example, the net-proton multiplicity distribution, which has been suggested as a sensitive signal for the QCD critical point [11–13], is strongly influenced by both volume fluctuations and charge conservations, which result in deviations from the Skellam distribution [33–36]. To impose strict charge conservations in the hybrid model simulations for QGP and hadronic evolution turns out to be difficult because the local correlation length between a charged particle pair is finite and is sensitive to the expansion of the produced fireball [40, 41]. It is thus highly nontrivial to include all of the important effects originated from non-critical fluctuations in a single model and calculate their contributions to the higher-order cumulants and the cumulant ratio of net-proton multiplicity distribution.

Recently, the STAR Collaboration has collected a wealth of data on light nuclei, such as (anti-)deuteron (\bar{d} , d), (anti-)triton (\bar{t} , t) and (anti-)helium-3 (${}^3\bar{He}$, 3He), and has also analyzed the energy dependence of their yields and yield ratios in heavy ion collisions at RHIC BES energies [31, 42–44]. The observed coalescence parameters of (anti-)deuteron ($B_2(d)$ and $B_2(\bar{d})$) and the yield ratio of light nuclei, $N_t N_p / N_d^2$, both show a clear non-monotonic energy dependence with a dip and a peak around $\sqrt{s_{NN}} = 20$ GeV in central Au+Au collisions, respectively [31, 44], implying a dramatic change of the speed of sound and a large relative density fluctuations of

nucleons associated with the QCD critical point [39, 45–49]. For a better understanding of these observables and evaluate their relations to critical behaviors, it is necessary and timely to carry out baseline calculations without including any effects from critical fluctuations.

In this paper, we study the collision energy dependence of light nuclei production at the RHIC BES energies based on the nucleon coalescence model using the nucleon phase-space distributions that do not contain any critical fluctuation effects. More specifically, nucleons are first thermally produced and evolved to the kinetic freeze-out of an expanding fireball described by the integrated hybrid approach iEBE-MUSIC with dynamical initial conditions that have been specifically developed for heavy ion collisions at the RHIC BES program. [50–54]. With the obtained phase-space distributions of protons and neutrons, we then implement the nucleon coalescence model to calculate the yields of light nuclei [55–58]. Compared to previous studies based on the thermal model or a transport model without the partonic phase [39, 45–48], our present hybrid model provides a more realistic calculation for light nuclei production without the effect of the QCD critical point, which can thus serve as more reliable baseline results for the related measurements in the experiments carried out in the RHIC BES program to search for the QCD critical point.

This paper is organized as the following: Section II briefly introduces the nucleon coalescence model and the iEBE-MUSIC hybrid model. Section III presents and discusses results on the collision energy dependence of the spectra and yield dN/dy of various hadrons and light nuclei, the coalescence parameters of (anti-)deuterons and (anti-)tritons, and the particle yield ratios in the most central Au+Au collisions at RHIC BES energies. Section IV concludes the paper.

II. THE THEORETICAL FRAMEWORK

A. The coalescence model for light nuclei production

In the coalescence model [55–58], light nuclei are produced by combining nucleons at their kinetic freeze-out with probabilities calculated in the sudden approximation. The production probability for a (anti-)nucleus of atomic number A consisting of Z (anti-)protons and N (anti-)neutrons ($A = Z + N$) is given by the overlap of the Wigner function f_A of the nucleus with the phase-space distributions $f_{p/\bar{p}}(\mathbf{x}_i, \mathbf{p}_i, t)$ of (anti-)proton

and $f_{n/\bar{n}}(\mathbf{x}_j, \mathbf{p}_j, t)$ of (anti-)neutrons [57, 58]:

$$\begin{aligned} \frac{dN_A}{d^3\mathbf{P}_A} &= \frac{g_A}{Z!N!} \int \prod_{i=1}^Z p_i^\mu d^3\sigma_{i\mu} \frac{d^3\mathbf{p}_i}{E_i} f_{p/\bar{p}}(\mathbf{x}_i, \mathbf{p}_i, t_i) \\ &\times \int \prod_{j=1}^N p_j^\mu d^3\sigma_{j\mu} \frac{d^3\mathbf{p}_j}{E_j} f_{n/\bar{n}}(\mathbf{x}_j, \mathbf{p}_j, t_j) \\ &\times f_A(\mathbf{x}'_1, \dots, \mathbf{x}'_Z, \mathbf{x}'_1, \dots, \mathbf{x}'_N; \mathbf{p}'_1, \dots, \mathbf{p}'_Z, \mathbf{p}'_1, \dots, \mathbf{p}'_N; t') \\ &\times \delta^{(3)}\left(\mathbf{P}_A - \sum_{i=1}^Z \mathbf{p}_i - \sum_{j=1}^N \mathbf{p}_j\right), \end{aligned} \quad (1)$$

where $g_A = (2J_A + 1)/[\Pi_{i=1}^A (2J_i + 1)]$ is the statistical factor for A nucleons of spins J_i to form a nucleus of angular momentum J_A . The coordinate and momentum of the i -th nucleon in the fireball frame are denoted by \mathbf{x}_i and \mathbf{p}_i , respectively. Its coordinate \mathbf{x}'_i and momentum \mathbf{p}'_i in the Wigner function of the produced nucleus are obtained by Lorentz transforming the coordinate \mathbf{x}_i and momentum \mathbf{p}_i to the rest frame of the nucleus.

In this paper, we focus on investigating the collision energy dependence of the production of (anti-)deuterons and (anti-)tritons in the RHIC BES program. Following Ref. [57], the Wigner functions of (anti-)deuterons and (anti-)tritons are taken to have the forms [59]

$$f_2(\boldsymbol{\rho}, \mathbf{p}_\rho) = 8 \exp \left[-\frac{\boldsymbol{\rho}^2}{\sigma_\rho^2} - \mathbf{p}_\rho^2 \sigma_\rho^2 \right], \quad (2)$$

and

$$\begin{aligned} f_3(\boldsymbol{\rho}, \boldsymbol{\lambda}, \mathbf{p}_\rho, \mathbf{p}_\lambda) \\ = 8^2 \exp \left[-\frac{\boldsymbol{\rho}^2}{\sigma_\rho^2} - \frac{\boldsymbol{\lambda}^2}{\sigma_\lambda^2} - \mathbf{p}_\rho^2 \sigma_\rho^2 - \mathbf{p}_\lambda^2 \sigma_\lambda^2 \right], \end{aligned} \quad (3)$$

respectively. Here the relative coordinates $\boldsymbol{\rho}$ and $\boldsymbol{\lambda}$, and the relative momenta \mathbf{p}_ρ and \mathbf{p}_λ are defined as:

$$\begin{aligned} \boldsymbol{\rho} &= \frac{1}{\sqrt{2}}(\mathbf{x}'_1 - \mathbf{x}'_2), \quad \mathbf{p}_\rho = \sqrt{2} \frac{m_2 \mathbf{p}'_1 - m_1 \mathbf{p}'_2}{m_1 + m_2}, \\ \boldsymbol{\lambda} &= \sqrt{\frac{2}{3}} \left(\frac{m_1 \mathbf{x}'_1 + m_2 \mathbf{x}'_2}{m_1 + m_2} - \mathbf{x}'_3 \right), \\ \mathbf{p}_\lambda &= \sqrt{\frac{3}{2}} \frac{m_3(\mathbf{p}'_1 + \mathbf{p}'_2) - (m_1 + m_2)\mathbf{p}'_3}{m_1 + m_2 + m_3}, \end{aligned} \quad (4)$$

with m_i , \mathbf{x}'_i and \mathbf{p}'_i being the mass, coordinate and momentum of nucleon i , respectively. The width parameter σ_ρ in Eq. (2) is related to the root-mean-square charge radius of the nucleus of two constituent nucleons via [59]

$$\langle r_2^2 \rangle = \frac{3}{2} \frac{|Q_1 m_1^2 + Q_2 m_2^2|}{(m_1 + m_2)^2} \sigma_\rho^2 = \frac{3}{4} \frac{|Q_1 m_1^2 + Q_2 m_2^2|}{\omega m_1 m_2 (m_1 + m_2)} \quad (5)$$

with Q_1 and Q_2 being the charges of the two nucleons, which provides the relation $\sigma_\rho = 1/\sqrt{\mu_1 \omega}$ in terms of the oscillator frequency ω in the harmonic wave function and

the reduced mass $\mu_1 = 2(1/m_1 + 1/m_2)^{-1}$. The width parameter σ_λ in Eq. (3) is related to the oscillator frequency by $\sigma_\lambda = 1/\sqrt{\mu_2\omega}$ with $\mu_2 = (3/2)[1/(m_1+m_2) + 1/m_3]^{-1}$. Similarly, its value is determined from the oscillator con-

stant via the root-mean-square charge radius of the nucleus with three constituent nucleons, which is expressed as [59]

$$\langle r_3^2 \rangle = \frac{1}{2} \frac{|Q_1 m_1^2(m_2 + m_3) + Q_2 m_2^2(m_3 + m_1) + Q_3 m_3^2(m_1 + m_2)|}{\omega(m_1 + m_2 + m_3)m_1 m_2 m_3}, \quad (6)$$

where Q_1 , Q_2 and Q_3 are the charges of the three nucleons.

For the production of triton, we consider the two production channels of $p + n + n \rightarrow t$ (3-body process) and $d + p \rightarrow t$ (2-body process). Here the deuteron in the latter process is treated as a point-like particle with its phase-space distribution given by that obtained from the coalescence of protons and neutrons. Note that the final triton yield is the summation over the 2-body and 3-body processes under the assumption that the coalescence processes occur instantaneously and monodirectionally [57, 58]. Alternatively, if one assumes that the triton yield in the coalescence model using nucleons from a thermally and chemically equilibrated emission source is the same as in the statistical model with the triton binding energy neglected, then the two coalescence processes $p+n+n \rightarrow t$ and $d+p \rightarrow t$ would give the same triton yield [45]. In this case, only one of the two processes should be considered in the coalescence model. In this work, we will quantify triton production from the 2-body and 3-body processes separately. Because of the very small number of (anti-)deuterons and tritons produced in heavy ion collisions, the protons and anti-protons participating in the coalescence processes have negligible effects in calculating the final (anti-)proton spectra.

TABLE I provides the statistical factors and the values of the width parameters in the Wigner functions for deuterons and tritons as well as the empirical values of their charge radii and the resulting oscillator constants.

TABLE I: Statistical factor (g), charge radius (R), oscillator frequency (ω) and width parameter (σ_ρ , σ_λ) for (anti-)deuteron and (anti-)triton. Charge radii are taken from Ref. [60].

Nucleus	g	R (fm)	ω (sec $^{-1}$)	$\sigma_\rho, \sigma_\lambda$ (fm)
$p + n \rightarrow \text{deuteron}$	3/4	2.1421	0.1739	2.473
$p + n + n \rightarrow \text{triton}$	1/4	1.7591	0.3438	1.759
$d + n \rightarrow \text{triton}$	1/3	1.7591	0.2149	1.927

B. The iEBE-MUSIC hybrid model for collision dynamics and particle production

For the phase-space distributions of (anti-)protons and (anti-)neutrons used in the coalescence model calculations of light (anti-)nuclei production at RHIC BES energies, we employ the iEBE-MUSIC hybrid model [61] to describe the collision dynamics until the kinetic freeze-out. iEBE-MUSIC is a generic event generator to simulate the QGP collective dynamics and soft hadrons production in relativistic heavy-ion collisions. At the RHIC BES energies, this hybrid model uses a 3D Monte-Carlo (MC) Glauber initial condition to dynamically deposit energy, momentum, and net baryon densities into the evolving fluid system as the two colliding nuclei are penetrating through each other [50, 52]. The collective expansion of the QGP fireball and the evolution of the conserved net-baryon current are simulated by a (3+1)D viscous hydrodynamic model MUSIC [53, 62–65]. As the QGP expands and transitions to the dilute hadronic phase, the fluid dynamic description is switched to a microscopic hadron cascade model, UrQMD [66–68], to simulate the succeeding evolution and decoupling of the hadronic matter.

More specifically, the dynamical initial condition is simulated by the 3D Monte-Carlo Glauber model on an event-by-event basis [50], and the space-time and momentum distributions of the initial energy-momentum tensor and net baryon charge current are provided by the classical string deceleration model [50, 69]. In order to reproduce the pseudo-rapidity distributions of charged hadrons for Au+Au Collisions at $\sqrt{s_{\text{NN}}} = 7.7 - 200$ GeV, we use the parameterized rapidity loss function given in Ref. [54]. We further introduce additional baryon charge fluctuations according to the string junction model [70, 71], which helps to achieve a good description of the measured rapidity distributions of net protons. The detailed implementation of this initial condition model and systematic phenomenological impacts will be reported in an upcoming work [71].

With such dynamical initial conditions, the hydrodynamic equations for the evolution of the energy-momentum tensor and the net baryon current are then solved with the inclusion of source terms [50]. Here we use the crossover equation of state (NEOS-BQS) for the QCD matter at finite chemical potentials, potentials that

is constructed from recent lattice [72–76]. This EoS is obtained by imposing the strangeness neutrality condition of vanishing net strangeness density, $n_s = 0$, and setting the net electric charge-to-baryon density ratio to $n_Q/n_B = 0.4$ [76]. Note that this EoS does not contain a QCD critical point since the model calculations in this paper aim to provide clean baseline results without any effects from critical fluctuations for the related measurements of light nuclei at the RHIC BES program. We leave the study of the influence of a critical point or critical fluctuations to future works. Following Refs. [54, 76], we only consider the shear viscous effects in the hydrodynamic evolution with the specific shear viscosity set to a constant value $\frac{\eta T}{e+P} = 0.08$. The shear stress tensor is evolved according to a set of relaxation type of equations up to the second order in spatial gradients [53, 77]. For simplicity, the effects from bulk viscosity and charge diffusion are neglected in this work.

In iEBE-MUSIC, the Cooper-Frye particlization of the fluid cells is performed on a hyper-surface with a constant energy density of $e_{sw} = 0.26$ GeV/fm³ using the open-source code package iSS [78, 79]. The produced hadrons are then fed into the hadron cascade model, UrQMD, for further scatterings and decays until their kinetic freeze-outs. Finally, we obtain the freeze-out phase-space distributions of nucleons for the coalescence model calculations.

A quantitative coalescence model calculation for light nuclei production requires realistic phase-space distributions of nucleons at the kinetic freeze-out [82, 83]. Therefore, it is necessary to achieve a good description of the identified particle $\langle p_T \rangle$ and p_T -spectra. Here, we emphasize that the iEBE-MUSIC hybrid model employed in this paper can capture both the longitudinal and transverse dynamics of the collision system. This hybrid model has achieved a consistent description of soft particle production in the most central Au-Au collisions at $\sqrt{s_{NN}} = 7.7 - 200$ GeV, as demonstrated in Ref. [54, 84] and Fig. 5 in the Appendix. The description of various flow observables within the iEBE-MUSIC hybrid model will be reported in the upcoming works [71].

III. RESULTS

In this section, we study the transverse momentum spectra and particle yield dN/dy at mid-rapidity, coalescence parameters $A^{-1}\sqrt{B_A}$ ($A = 2, 3$) and yield ratios of light (anti-)nuclei in 0-10% Au+Au collisions at $\sqrt{s_{NN}} = 7.7, 11.5, 19.6, 27, 39, 62.4$, and 200 GeV. Simulation results are calculated from the coalescence model using the phase-space distributions of (anti-)protons and (anti-)neutrons generated from the iEBE-MUSIC hybrid model.

A. Transverse Momentum Spectra and dN/dy

Figure 1 shows the transverse momentum spectra of (anti-)protons, (anti-)deuterons and tritons in the most central (0-10%)¹ Au + Au collisions at $\sqrt{s_{NN}} = 7.7, 11.5, 19.6, 27, 39, 62.4$, and 200 GeV. For the spectra of protons and anti-protons², the iEBE-MUSIC hybrid model gives a quantitative description of the measured data below 2.5 GeV, but slightly underestimates the data above 3 GeV. At the high p_T region, the quark recombination process [85–90], not included in the Cooper-Frye particlization, gradually becomes important. With the phase-space distributions of (anti-)protons and (anti-)neutrons at kinetic freeze-out, we calculate the spectra of (anti-)deuterons and tritons using the nucleon coalescence model. As shown with the blue solid and dotted lines in Fig. 1, our model calculations nicely reproduce the p_T -spectra of deuterons and anti-deuterons measured by the STAR Collaboration over a wide range of collision energies. The good theoretical descriptions extend to higher p_T at higher collision energies as a result of the stronger hydrodynamic radial flow. The transverse momentum spectra of tritons are calculated using both the $p + n + n \rightarrow t$ (3-body) and the $d + p \rightarrow t$ (2-body) coalescence processes. Our results from the 3-body process reasonably describe the STAR data in Au+Au collisions at $\sqrt{s_{NN}} = 7.7 - 39$ GeV. Including the additional 2-body channel would overestimate the triton yield by a factor of 2. Hence our calculations indicate that triton yield at RHIC BES is close to the thermal equilibrium, consistent with the expectation from the statistical model [91, 92]. At $\sqrt{s_{NN}} = 62.4$ and 200 GeV, the slopes of the calculated triton p_T -spectra are slightly harder than those of the measured ones, which might be caused by the stronger radial flow at $\sqrt{s_{NN}} = 62.4$ and 200 GeV in our model calculations.

Figure 2a shows the dependence of the mid-rapidity particle yields for (anti-)protons, (anti-)deuterons, and (anti-)tritons on collision energy. Our simulations quantitatively reproduce the STAR measurements within 10%. The final proton yields are larger at lower collision energies because of the interplay between the effects of baryon charge transport and the thermal production of nucleons. The 3D MC-Glauber model, with the dynamical initialization scheme and string junction fluctuations for net baryon charges gives a realistic estimation of initial

¹ Here, we cut the centrality bins in iEBE-MUSIC calculations according to the impact parameter b in the initial state. The upper limits for b are 4.60 fm, 4.61 fm, 4.62 fm, 4.65 fm, 4.67 fm, 4.68 fm, and 4.70 fm for 0-10% Au+Au collisions at $\sqrt{s_{NN}} = 7.7, 11.5, 19.6, 27, 39, 62.4$, and 200 GeV, respectively.

² The data on (anti-)protons for Au+Au collisions at $\sqrt{s_{NN}} = 7.7 - 62.4$ GeV are taken from the STAR measurements [80] and those at $\sqrt{s_{NN}} = 200$ GeV are taken from the PHENIX measurements [81]. All data have been corrected by subtracting the feed-down contributions from hyperon weak decays.

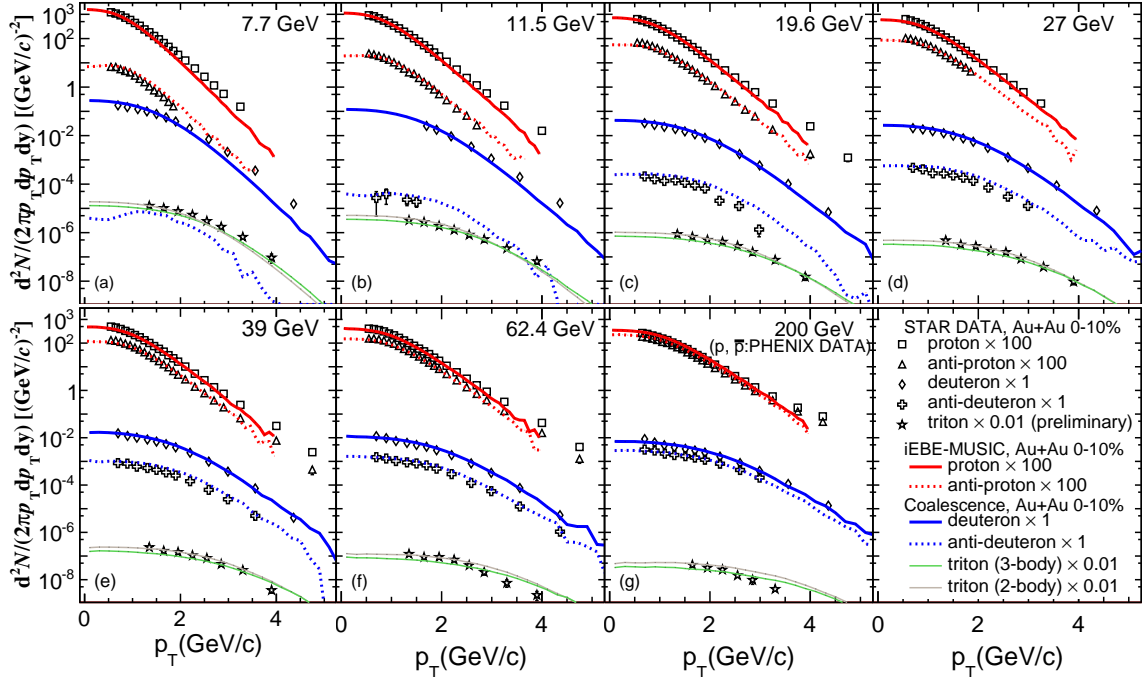


FIG. 1: (Color online) Transverse momentum spectra of (anti-)protons, (anti-)deuterons and tritons in 0-10% Au + Au collisions at $\sqrt{s_{NN}} = 7.7, 11.5, 19.6, 27, 39, 62.4$, and 200 GeV. The data for (anti-)deuterons and tritons are taken from the STAR Collaboration [31, 44, 80], and the data for (anti-)protons are taken from the STAR and PHENIX Collaborations [81].

baryon stopping. For the proton yields at lower collision energies, the contributions from the initial baryon stopping and baryon current evolution during the hydrodynamic phase gradually overwhelms those from the thermal production at particlization. The calculated dN/dy of deuterons, (anti-)deuterons, tritons, and (anti-)tritons also show a similar dependence on the collision energy, which again gives a reasonable description of the STAR data.

Figure 2b shows the energy dependence of the yield ratios of light (anti-)nuclei to (anti-)protons. In general, these calculated ratios agree with the measured data in the most central Au+Au collisions at $\sqrt{s_{NN}} = 7.7 - 200$ GeV within a 20% accuracy. Our calculation overestimates the d/p and \bar{d}/\bar{p} ratios by 15% and 20%, respectively. The coalescence model nicely reproduces the t/p ratios with tritons produced from the 3-body process, while underestimates the t/d ratios by 10%.

B. Coalescence Parameters and Light Nuclei Yield Ratios

In the coalescence picture, the invariant yield of light nuclei with the mass number $A = Z + N$ is proportional to the invariant yields of protons and neutrons according

to

$$E_A \frac{d^3 N_A}{dp_A^3} = B_A \left(E_p \frac{d^3 N_p}{dp_p^3} \right)^Z \left(E_n \frac{d^3 N_n}{dp_n^3} \right)^{A-Z} \approx B_A \left(E_p \frac{d^3 N_p}{dp_p^3} \right)^A \Big|_{\vec{p}_p = \vec{p}_n = \frac{\vec{p}_A}{A}}, \quad (7)$$

where $\vec{p}_{p,n}$ are the proton and neutron momenta and $E_{p,n}$ are their energies. The coalescence parameter B_A characterizes the coalescence probability and is related to the effective volume, V_{eff} , of the hadronic emission source [93–95],

$$B_A \propto V_{\text{eff}}^{1-A}. \quad (8)$$

Figure 3 shows the collision energy dependence of the coalescence parameters $B_2(d)$, $B_2(\bar{d})$ and $\sqrt{B_3(t)}$ at $p_T/A=0.65$ GeV in the most central Au+Au collisions, with $A = 2$ for (anti-)deuterons and $A = 3$ for tritons. The measured $B_2(d)$ and $B_2(\bar{d})$ from the STAR collaboration [44] show a non-monotonic dependence on the collision energy with a dip located around $\sqrt{s_{NN}} = 20 - 40$ GeV, which might indicate a dramatic change of the equation of state in the produced matter at these collision energies [30, 44]. In contrast, our coalescence model calculations, using the phase-phase distributions of protons and neutrons generated from the iEBE-MUSIC hybrid model with a crossover EoS in the hydrodynamics, gives a monotonically decreasing $B_2(d)$ and $B_2(\bar{d})$, which is because the overall sizes of the emitting source of nucleons increases monotonically with the collision energy in our

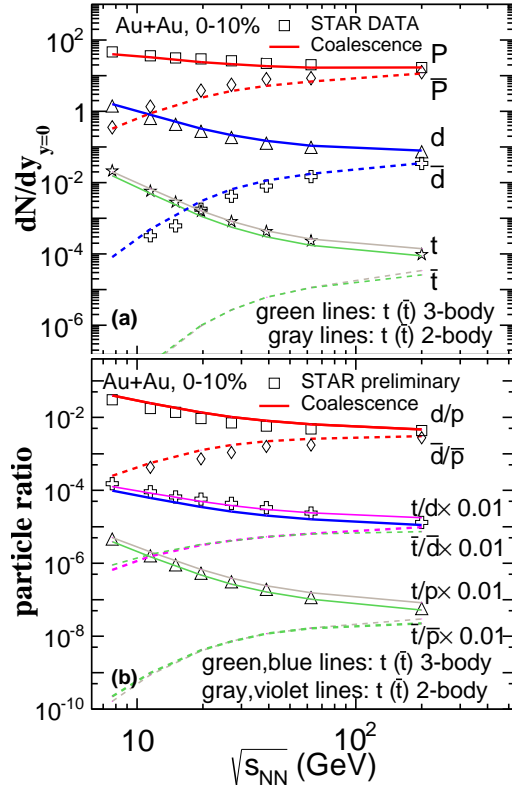


FIG. 2: (Color online) Collision energy dependence of (a) dN/dy of (anti-)protons, (anti-)deuterons, and (anti-)tritons at mid-rapidity and (b) the particle ratio d/p , \bar{d}/\bar{p} , t/d , \bar{t}/\bar{d} , t/p and \bar{t}/\bar{p} in 0-10% Au + Au collisions. The experimental data for (anti-)protons, (anti-)deuterons, and tritons are taken from [31, 44, 80, 81].

model. Also, our model overestimates the values $B_2(d)$ and $B_2(\bar{d})$ by $\sim 50\%$ for $\sqrt{s_{NN}} = 20 - 62.4$ GeV, because our calculations overestimate the yield of deuterons by 10% while underestimate the proton yield by 15%. The relative ratios between proton and deuteron yields are sensitive to the phase-space distribution of nucleons at the kinetic freeze-out. Therefore, the experimental measurements of $B_2(d)$ and $B_2(\bar{d})$ can set strong constraints on the spatial-momentum correlations of nucleons in the hadronic phase. In addition, the measured $B_2(d)$ and $B_2(\bar{d})$ curves as functions of the collision energy show a clear separation, while these curves from our calculations almost overlap. We note that these coalescence parameters have recently also been studied in Ref. [96] by using the hydrodynamics + SMASH hadronic transport model with event-averaged 3D initial conditions based on collision geometry [97]. Instead of production from nucleon coalescence, (anti-)deuterons in this study are treated as dynamic degrees of freedom through the pion catalysis reactions $\pi d \leftrightarrow \pi p N$ with large cross sections. The resulting (anti-)deuteron yields and spectra were studied for the most central Au+Au collisions at $\sqrt{s_{NN}} = 7 - 200$ GeV. It is pointed out in this study that the weak decay corrections to the proton spectrum need careful attention

as they could potentially lead to a minimum in the collision energy dependence of the coalescence parameters $B_2(d)$ and $B_2(\bar{d})$.

As expected from Eq. (8), the calculated $\sqrt{B_3(t)}$ curve shows a similar trend as the $B_2(d)$ curve, which monotonically increases with the decrease of the collision energy. This is also consistent with the calculated flat yield ratio $N_t N_p / N_d^2$ described below. Note that our coalescence model calculations with the 3-body process roughly describe the magnitude of the measured $\sqrt{B_3(t)}$ curve in the most central Au + Au collisions at $\sqrt{s_{NN}} = 7.7 - 200$ GeV, but not the non-monotonic behavior. In our calculations, the values of $B_2(\bar{d}/d)$ are larger than those of $\sqrt{B_3(t)}$, which suggests that tritons and deuterons are produced with different degrees of sensitivity to the nucleon phase-space distributions in the coalescence process. Including triton production from the 2-body coalescence process increases the values of $\sqrt{B_3(t)}$, which makes them closer to the values of $B_2(\bar{d}/d)$ in our calculations.

Recently, the yield ratio of light nuclei, $N_t N_p / N_d^2$, in heavy ion collisions has been suggested as a sensitive probe to the neutron density fluctuation associated with the first-order QGP to hadronic matter phase transition and the possible critical point of the hot and baryon-rich QCD matter [45, 46, 98, 99]. Figure 4 shows the $N_t N_p / N_d^2$ ratio as a function of the collision energy from the experiments by the STAR Collaboration and from our coalescence model calculations. The measured $N_t N_p / N_d^2$ ratio shows a non-monotonic behavior with a peak located around $\sqrt{s_{NN}} = 20$ GeV [31], which might indicate a non-trivial collision energy dependence of the baryon density fluctuations [45, 46]. In contrast, the calculated $N_t N_p / N_d^2$ ratios for both cases of 2-body and 3-body coalescence processes are almost flat in their collision energy dependence, and this is due to the absence of any non-trivial baryon density fluctuations associated with the critical point as a result of using a crossover type

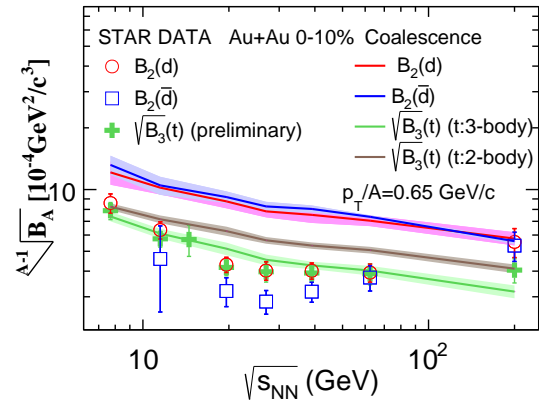


FIG. 3: (Color online) Collision energy dependence of the coalescence parameters $B_2(d)$, $B_2(\bar{d})$ and $\sqrt{B_3(t)}$ at $p_T/A = 0.65$ GeV in 0-10% Au+Au collisions, calculated by the coalescence model. The values extracted from the experimental data for $B_2(d)$, $B_2(\bar{d})$ and $B_3(t)$ are taken from [31, 44].

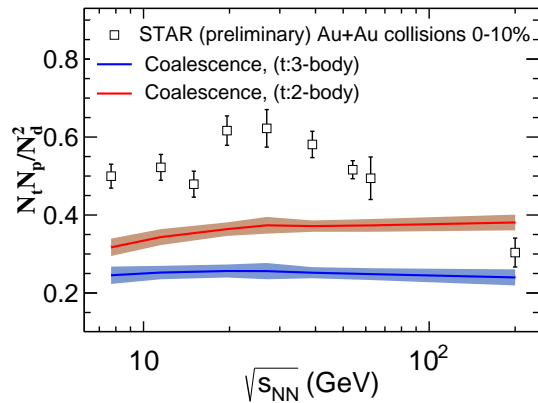


FIG. 4: (Color online) Collision energy dependence of the yield ratio $N_t N_p / N_d^2$ in 0-10% Au+Au collisions calculated from the coalescence model. The data is taken from Ref. [31].

EoS in the iEBE-MUSIC hybrid model. As to the yield ratio $N_t N_p / N_d^2$, the two-body process slightly overestimates whereas the three-body process slightly underestimates the measured value at 200 GeV. Both processes greatly underestimate, however, the measured value at $\sqrt{s_{NN}} \leq 62.4$ GeV.

Figure 4 further shows that the yield ratio $N_t N_p / N_d^2$ with tritons produced from the 2-body process is larger than that with tritons produced from the 3-body process in our model, which is a consequence of the non-trivial spatial-momentum correlations in the nucleon phase-space distributions from our iEBE-MUSIC hybrid model. It is shown in Ref. [100] that the yield ratios from these two processes would be the same if the nucleon phase-space distributions are uniform in the coordinate space. We emphasize that our model does not contain any effects from a critical point, which thus provides the non-critical baseline results for the yields of these light nuclei in heavy ion collisions at the RHIC BES energies. For a better explanation of the observed non-monotonic behavior of $N_t N_p / N_d^2$, $B_2(d)$, $B_2(\bar{d})$ and $\sqrt{B_3(t)}$ in their collision energy dependence, a dynamical model with critical fluctuations or the effects of critical point is required.

We note that our result on the yield ratio $N_t N_p / N_d^2$ is similar to those found in Ref. [39], which is based on a simple phase-space coalescence model using nucleons from the JAM hadronic cascade model [101] and in Ref. [48], which is based on a coalescence model similar to that in the present study with nucleons from a multi-phase transport (AMPT) model [102].

Although a non-monotonic collision energy dependence of the yield ratio $N_t N_p / N_d^2$ has been reported in Ref. [49] from a coalescence model study using nucleons from the UrQMD model [66], the result is puzzling because of the unexpected very different nucleon and light nuclei rapidity distributions predicted from this study.

IV. SUMMARY

In this paper, we have used the nucleon coalescence model to study light nuclei production in the most central Au+Au collisions at $\sqrt{s_{NN}} = 7.7, 11.5, 19.6, 27, 39, 62.4$ and 200 GeV. The input phase-space distributions of (anti-)protons and (anti-)neutrons at kinetic freeze-out for the coalescence calculations are generated from the iEBE-MUSIC hybrid model using three dimensional dynamical initial conditions and a crossover EoS. These comprehensive simulations can nicely reproduce the measured p_T -spectra of (anti-)pions, (anti-)kaons, and (anti-)protons for Au+Au collisions at $\sqrt{s_{NN}} = 7.7 - 200$ GeV (as shown in the appendix and in Ref. [84]). We have found that the subsequent coalescence model calculations can reproduce the measured p_T -spectra and dN/dy of (anti-)deuterons and (anti-)tritons and the particle ratios of t/p within 10% of accuracy. However, the deviations between the calculated and measured particle ratios of d/p , \bar{d}/\bar{p} , and t/d increase to 15%, 20%, and 10%, respectively.

Although the coalescence model reasonably describes the p_T -spectra and yields of light nuclei at various collision energies, the predicted coalescence parameters of (anti-)deuterons and tritons, $B_2(d)$, $B_2(\bar{d})$ and $\sqrt{B_3(t)}$, decrease monotonically with increasing collision energy, and the yield ratio $N_t N_p / N_d^2$ stays almost constant with respect to the collision energy. All these theoretical results fail to describe the non-monotonic behavior of the corresponding measurements in experiments. We emphasize that the hydrodynamic part of our calculations with a crossover EoS for all collision energies does not generate any dynamical density fluctuations, which are related to the critical point and first-order phase transition, for the subsequent nucleon coalescence model calculations. According to Refs. [45, 46], non-trivial density fluctuations in the produced hot QCD matter are needed to describe this non-monotonic behavior. Our model calculations thus provide the non-critical baseline results for comparisons with related light nuclei measurements at the RHIC BES program. We leave the implementation of an EoS with a critical point in the hydrodynamic evolution and the inclusion of dynamical density fluctuations to future studies.

Acknowledgements

We thank X. F. Luo, N. Yu and D. W. Zhang for providing the STAR data as well as K. Murase, D. Oliinchenko, K. J. Sun and S. Wu for discussions. W. Z., Q. L. and H. S. are supported by the NSFC under grant Nos. 11675004. C. S. is supported in part by the U.S. Department of Energy (DOE) under grant number DE-SC0013460 and in part by the National Science Foundation (NSF) under grant number PHY-2012922. C.M. K. is supported by US DOE under Award No. DE-SC0015266 and the Welch Foundation under Grant No.

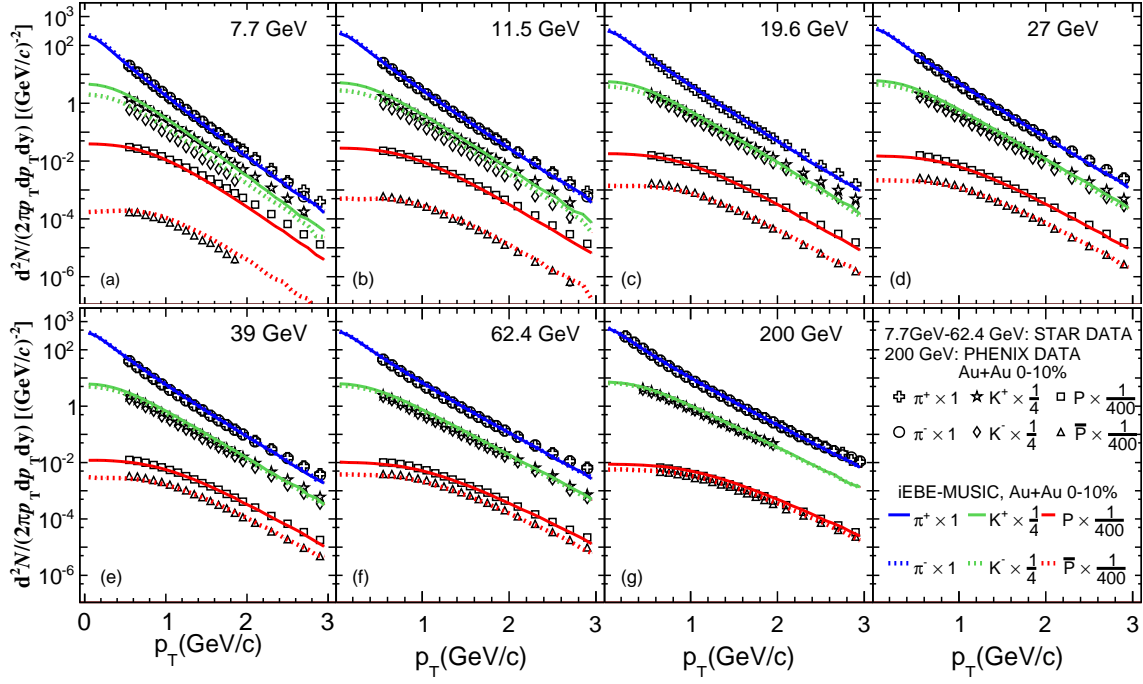


FIG. 5: (Color online) Transverse momentum spectra of (anti-)pions, (anti-)kaons, and (anti-)protons in 0-10% Au + Au collisions at $\sqrt{s_{NN}} = 7.7, 11.5, 19.6, 27, 39, 62.4,$ and 200 GeV, calculated from the iEBE-MUSIC hybrid model. The data are taken from the STAR and PHENIX Collaborations [80, 81].

A-1358. This work is also supported in part by the U.S. Department of Energy, Office of Science, Office of Nuclear Physics, within the framework of the Beam Energy Scan Theory (BEST) Topical Collaboration. C. S further acknowledge computing resources of the National Energy Research Scientific Computing Center, which is supported by the Office of Science of the U.S. Department of Energy under Contract No. DE-AC02-05CH11231. W. Z. and H. S. also gratefully acknowledge the extensive computing resources provided by the Super-computing Center of Chinese Academy of Science (SCCAS), Tianhe-1A from the National Supercomputing Center in Tianjin, China and the High-performance Computing Platform of Peking University.

Appendix: p_T -spectra of (anti-)pions, (anti-)kaons and (anti-)protons

In this appendix, we present the iEBE-MUSIC hybrid model calculations using the dynamical initialization and

string junction fluctuations for net baryon charges to study the p_T -spectra of (anti-)pions, (anti-)kaons, and (anti-)protons in 0-10% central Au + Au collisions at $\sqrt{s_{NN}} = 7.7, 11.5, 19.6, 27, 39, 62.4,$ and 200 GeV. Figure 5 shows that this model gives a good description of the p_T -spectra of these identified hadrons. Such quantitative descriptions, especially for the p_T spectra of protons and anti-protons, demonstrates that this three-dimensional hybrid model, without any critical fluctuations, can provide a reliable phase-space distributions of nucleons for the subsequent coalescence model calculations of light nuclei production at various collision energies in the RHIC BES program.

-
- [1] M. A. Stephanov, Prog. Theor. Phys. Suppl. **153**, 139 (2004), [Int. J. Mod. Phys.A20,4387(2005)], hep-ph/0402115.
 - [2] M. Stephanov, PoS **LAT2006**, 024 (2006), hep-lat/0701002.
 - [3] Y. Aoki, G. Endrodi, Z. Fodor, S. D. Katz, and K. K.

- Szabo, Nature **443**, 675 (2006), hep-lat/0611014.
- [4] M. Aggarwal et al. (STAR) (2010), 1007.2613.
- [5] K. Fukushima and T. Hatsuda, Rept. Prog. Phys. **74**, 014001 (2011), 1005.4814.
- [6] Y. Akiba et al. (2015), 1502.02730.
- [7] U. Heinz et al. (2015), 1501.06477.

- [8] M. Asakawa and M. Kitazawa, *Prog. Part. Nucl. Phys.* **90**, 299 (2016), 1512.05038.
- [9] X. Luo and N. Xu, *Nucl. Sci. Tech.* **28**, 112 (2017), 1701.02105.
- [10] A. Bzdak, S. Esumi, V. Koch, J. Liao, M. Stephanov, and N. Xu (2019), 1906.00936.
- [11] M. A. Stephanov, *Phys. Rev. Lett.* **102**, 032301 (2009), 0809.3450.
- [12] M. Stephanov, *Phys. Rev. Lett.* **107**, 052301 (2011), 1104.1627.
- [13] C. Athanasiou, K. Rajagopal, and M. Stephanov, *Phys. Rev. D* **82**, 074008 (2010), 1006.4636.
- [14] M. Asakawa, S. Ejiri, and M. Kitazawa, *Phys. Rev. Lett.* **103**, 262301 (2009), 0904.2089.
- [15] M. Nahrgang, S. Leupold, C. Herold, and M. Bleicher, *Phys. Rev. C* **84**, 024912 (2011), 1105.0622.
- [16] B. Ling and M. A. Stephanov, *Phys. Rev. C* **93**, 034915 (2016), 1512.09125.
- [17] L. Jiang, P. Li, and H. Song, *Phys. Rev. C* **94**, 024918 (2016), 1512.06164.
- [18] L. Jiang, S. Wu, and H. Song, *Nucl. Phys. A* **967**, 441 (2017), 1704.04765.
- [19] S. Mukherjee, R. Venugopalan, and Y. Yin, *Phys. Rev. C* **92**, 034912 (2015), 1506.00645.
- [20] S. Mukherjee, R. Venugopalan, and Y. Yin, *Phys. Rev. Lett.* **117**, 222301 (2016), 1605.09341.
- [21] M. Stephanov and Y. Yin, *Phys. Rev. D* **98**, 036006 (2018), 1712.10305.
- [22] M. Sakaida, M. Asakawa, H. Fujii, and M. Kitazawa, *Phys. Rev. C* **95**, 064905 (2017), 1703.08008.
- [23] S. Borsanyi, Z. Fodor, J. N. Guenther, S. K. Katz, K. K. Szabo, A. Pasztor, I. Portillo, and C. Ratti, *JHEP* **10**, 205 (2018), 1805.04445.
- [24] Y. Akamatsu, D. Teaney, F. Yan, and Y. Yin, *Phys. Rev. C* **100**, 044901 (2019), 1811.05081.
- [25] M. Nahrgang, M. Bluhm, T. Schaefer, and S. A. Bass, *Phys. Rev. D* **99**, 116015 (2019), 1804.05728.
- [26] G. Odyniec (STAR), *PoS CORFU2018*, 151 (2019).
- [27] X. Luo (STAR), *PoS CPOD2014*, 019 (2015), 1503.02558.
- [28] K. Aamodt et al. (ALICE), *Phys. Lett. B* **696**, 328 (2011), 1012.4035.
- [29] L. Adamczyk et al. (STAR), *Phys. Rev. C* **92**, 014904 (2015), 1403.4972.
- [30] R. A. Lacey, *Phys. Rev. Lett.* **114**, 142301 (2015), 1411.7931.
- [31] D. Zhang (STAR) (2019), 1909.07028.
- [32] F. Karsch and K. Redlich, *Phys. Lett. B* **695**, 136 (2011), 1007.2581.
- [33] S. Borsanyi, Z. Fodor, S. D. Katz, S. Krieg, C. Ratti, and K. K. Szabo, *Phys. Rev. Lett.* **111**, 062005 (2013), 1305.5161.
- [34] X. Luo, B. Mohanty, and N. Xu, *Nucl. Phys. A* **931**, 808 (2014), 1408.0495.
- [35] P. K. Netrakanti, X. F. Luo, D. K. Mishra, B. Mohanty, A. Mohanty, and N. Xu, *Nucl. Phys. A* **947**, 248 (2016), 1405.4617.
- [36] J. Li, H.-j. Xu, and H. Song, *Phys. Rev. C* **97**, 014902 (2018), 1707.09742.
- [37] S. He, X. Luo, Y. Nara, S. Esumi, and N. Xu, *Phys. Lett. B* **762**, 296 (2016), 1607.06376.
- [38] J. Xu, S. Yu, F. Liu, and X. Luo, *Phys. Rev. C* **94**, 024901 (2016), 1606.03900.
- [39] H. Liu, D. Zhang, S. He, N. Yu, and X. Luo (2019), 1909.09304.
- [40] S. Pratt and C. Plumberg, *Phys. Rev. C* **99**, 044916 (2019), 1812.05649.
- [41] D. Oliinychenko and V. Koch, *Phys. Rev. Lett.* **123**, 182302 (2019), 1902.09775.
- [42] L. Adamczyk et al. (STAR), *Phys. Rev. C* **94**, 034908 (2016), 1601.07052.
- [43] J. Chen, D. Keane, Y.-G. Ma, A. Tang, and Z. Xu, *Phys. Rept.* **760**, 1 (2018), 1808.09619.
- [44] J. Adam et al. (STAR), *Phys. Rev. C* **99**, 064905 (2019), 1903.11778.
- [45] K.-J. Sun, L.-W. Chen, C. M. Ko, and Z. Xu, *Phys. Lett. B* **774**, 103 (2017), 1702.07620.
- [46] K.-J. Sun, L.-W. Chen, C. M. Ko, J. Pu, and Z. Xu, *Phys. Lett. B* **781**, 499 (2018), 1801.09382.
- [47] N. Yu, D. Zhang, and X. Luo, *Chin. Phys. C* **44**, 014002 (2020), 1812.04291.
- [48] K.-J. Sun and C. M. Ko (2020), 2005.00182.
- [49] X. G. Deng and Y. G. Ma (2020), 2006.12337.
- [50] C. Shen and B. Schenke, *Phys. Rev. C* **97**, 024907 (2018), 1710.00881.
- [51] C. Shen and B. Schenke, *PoS CPOD2017*, 006 (2018), 1711.10544.
- [52] The 3D Monte-Carlo Glauber Model is a code package to simulate high-energy nucleus-nucleus collisions in 3D. The longitudinal energy-momentum distribution is based on the classical string deceleration model. This work uses v0.5 of this framework, which can be downloaded from <https://github.com/chunshen1987/3dMCGlauber>.
- [53] G. S. Denicol, C. Gale, S. Jeon, A. Monnai, B. Schenke, and C. Shen, *Phys. Rev. C* **98**, 034916 (2018), 1804.10557.
- [54] C. Shen and B. Schenke, *Nucl. Phys. A* **982**, 411 (2019), 1807.05141.
- [55] R. Mattiello, A. Jahns, H. Sorge, H. Stoecker, and W. Greiner, *Phys. Rev. Lett.* **74**, 2180 (1995).
- [56] R. Mattiello, H. Sorge, H. Stoecker, and W. Greiner, *Phys. Rev. C* **55**, 1443 (1997), nucl-th/9607003.
- [57] L.-W. Chen, C. M. Ko, and B.-A. Li, *Phys. Rev. C* **68**, 017601 (2003), nucl-th/0302068.
- [58] L.-W. Chen, C. M. Ko, and B.-A. Li, *Nucl. Phys. A* **729**, 809 (2003), nucl-th/0306032.
- [59] C. M. Ko, T. Song, F. Li, V. Greco, and S. Plumari, *Nucl. Phys. A* **928**, 234 (2014), 1211.5511.
- [60] I. Angeli and K. P. Marinova, *Atom. Data Nucl. Data Tabl.* **99**, 69 (2013).
- [61] The iEBE-MUSIC is a general-purpose numerical framework to simulate dynamical evolution of relativistic heavy-ion collisions event-by-event. This work uses v0.5 of this framework, which can be downloaded from <https://github.com/chunshen1987/iEBE-MUSIC>.
- [62] B. Schenke, S. Jeon, and C. Gale, *Phys. Rev. Lett.* **106**, 042301 (2011), 1009.3244.
- [63] B. Schenke, S. Jeon, and C. Gale, *Phys. Rev. C* **82**, 014903 (2010), 1004.1408.
- [64] J.-F. Paquet, C. Shen, G. S. Denicol, M. Luzum, B. Schenke, S. Jeon, and C. Gale, *Phys. Rev. C* **93**, 044906 (2016), 1509.06738.
- [65] MUSIC is the numerical implementation of (3+1)D relativistic viscous hydrodynamic simulations for high energy heavy-ion collisions. Its official website is <http://www.physics.mcgill.ca/music>. This work uses v2.5 of this framework, which can be downloaded from

- <https://github.com/MUSIC-fluid/MUSIC>.
- [66] S. A. Bass et al., Prog. Part. Nucl. Phys. **41**, 255 (1998), [Prog. Part. Nucl. Phys.41,225(1998)], nucl-th/9803035.
 - [67] M. Bleicher et al., J. Phys. **G25**, 1859 (1999), hep-ph/9909407.
 - [68] We use the official UrQMD v3.4 and set it up to run as the afterburner mode, https://bitbucket.org/Chunshen1987/urqmd_afterburner/src/master/.
 - [69] A. Bialas, A. Bzdak, and V. Koch, Acta Phys. Polon. **B49**, 103 (2018), 1608.07041.
 - [70] D. Kharzeev, Phys. Lett. **B378**, 238 (1996), nucl-th/9602027.
 - [71] C. Shen and B. Schenke, in preparation.
 - [72] S. Borsanyi, Z. Fodor, S. D. Katz, S. Krieg, C. Ratti, and K. Szabo, JHEP **01**, 138 (2012), 1112.4416.
 - [73] S. Borsanyi, Z. Fodor, C. Hoelbling, S. D. Katz, S. Krieg, and K. K. Szabo, Phys. Lett. **B730**, 99 (2014), 1309.5258.
 - [74] H. T. Ding, S. Mukherjee, H. Ohno, P. Petreczky, and H. P. Schadler, Phys. Rev. D **92**, 074043 (2015), 1507.06637.
 - [75] A. Bazavov et al., Phys. Rev. D **95**, 054504 (2017), 1701.04325.
 - [76] A. Monnai, B. Schenke, and C. Shen, Phys. Rev. **C100**, 024907 (2019), 1902.05095.
 - [77] G. Denicol, H. Niemi, E. Molnar, and D. Rischke, Phys. Rev. D **85**, 114047 (2012), [Erratum: Phys.Rev.D 91, 039902 (2015)], 1202.4551.
 - [78] C. Shen, Z. Qiu, H. Song, J. Bernhard, S. Bass, and U. Heinz, Comput. Phys. Commun. **199**, 61 (2016), 1409.8164.
 - [79] The iSS code package is an open-source particle sampler based on the Cooper-Frye freeze-out prescription. It converts fluid cells to particle samples. This work uses v1.0 of the iSS, which can be downloaded from <https://github.com/chunshen1987/iSS/releases>.
 - [80] L. Adamczyk et al. (STAR), Phys. Rev. Lett. **121**, 032301 (2018), 1707.01988.
 - [81] S. S. Adler et al. (PHENIX), Phys. Rev. **C69**, 034909 (2004), nucl-ex/0307022.
 - [82] W. Zhao, H.-j. Xu, and H. Song, Eur. Phys. J. **C77**, 645 (2017), 1703.10792.
 - [83] W. Zhao, L. Zhu, H. Zheng, C. M. Ko, and H. Song, Phys. Rev. **C98**, 054905 (2018), 1807.02813.
 - [84] C. Shen (2020), 2001.11858.
 - [85] V. Greco, C. M. Ko, and P. Levai, Phys. Rev. **C68**, 034904 (2003), nucl-th/0305024.
 - [86] V. Greco, C. M. Ko, and R. Rapp, Phys. Lett. **B595**, 202 (2004), nucl-th/0312100.
 - [87] R. J. Fries, B. Muller, C. Nonaka, and S. A. Bass, Phys. Rev. **C68**, 044902 (2003), nucl-th/0306027.
 - [88] R. C. Hwa and C. B. Yang, Phys. Rev. **C70**, 024905 (2004), nucl-th/0401001.
 - [89] R. J. Fries, V. Greco, and P. Sorensen, Ann. Rev. Nucl. Part. Sci. **58**, 177 (2008), 0807.4939.
 - [90] W. Zhao, C. M. Ko, Y.-X. Liu, G.-Y. Qin, and H. Song (2019), 1911.00826.
 - [91] A. Andronic, P. Braun-Munzinger, K. Redlich, and J. Stachel, Nature **561**, 321 (2018), 1710.09425.
 - [92] K.-J. Sun, C. M. Ko, F. Li, J. Xu, and L.-W. Chen (2020), 2006.08929.
 - [93] L. P. Csernai and J. I. Kapusta, Phys. Rept. **131**, 223 (1986).
 - [94] R. Scheibl and U. W. Heinz, Phys. Rev. **C59**, 1585 (1999), nucl-th/9809092.
 - [95] F. Bellini and A. P. Kalweit, Phys. Rev. **C99**, 054905 (2019), 1807.05894.
 - [96] D. Oliinychenko, C. Shen, and V. Koch (2020), 2009.01915.
 - [97] C. Shen and S. Alzhrani, Phys. Rev. C **102**, 014909 (2020), 2003.05852.
 - [98] E. Shuryak and J. M. Torres-Rincon, Phys. Rev. **C100**, 024903 (2019), 1805.04444.
 - [99] E. Shuryak and J. M. Torres-Rincon (2019), 1910.08119.
 - [100] K.-J. Sun, C. M. Ko, and B. Donigus, Phys. Lett. **B792**, 132 (2019), 1812.05175.
 - [101] Y. Nara, N. Otuka, A. Ohnishi, K. Niita, and S. Chiba, Phys. Rev. C **61**, 024901 (2000), nucl-th/9904059.
 - [102] Z.-W. Lin, C. M. Ko, B.-A. Li, B. Zhang, and S. Pal, Phys. Rev. C **72**, 064901 (2005), nucl-th/0411110.